

Quantifying the Uncertainty in Model Parameters using Gaussian Process-Based Markov Chain Monte Carlo: An Application to Cardiac Electrophysiological Models

Jwala Dhamala¹, John L. Sapp², Milan Horacek², and Linwei Wang¹

¹ Rochester Institute of Technology, Rochester, NY, 14623, USA

² Dalhousie University, Halifax, Canada

Abstract. Estimation of patient-specific model parameters is important for personalized modeling, although sparse and noisy clinical data can introduce significant uncertainty in the estimated parameter values. This importance source of uncertainty, if left unquantified, will lead to unknown variability in model outputs that hinder their reliable adoptions. Probabilistic estimation model parameters, however, remains an unresolved challenge because standard Markov Chain Monte Carlo sampling requires repeated model simulations that are computationally infeasible. A common solution is to replace the simulation model with a computationally-efficient surrogate for a faster sampling. However, by sampling from an approximation of the exact posterior probability density function (pdf) of the parameters, the efficiency is gained at the expense of sampling accuracy. In this paper, we address this issue by integrating surrogate modeling into Metropolis Hasting (MH) sampling of the exact posterior pdfs to improve its acceptance rate. It is done by first quickly constructing a Gaussian process (GP) surrogate of the exact posterior pdfs using deterministic optimization. This efficient surrogate is then used to modify commonly-used proposal distributions in MH sampling such that only proposals accepted by the surrogate will be tested by the exact posterior pdf for acceptance/rejection, reducing unnecessary model simulations at unlikely candidates. Synthetic and real-data experiments using the presented method show a significant gain in computational efficiency without compromising the accuracy. In addition, insights into the non-identifiability and heterogeneity of tissue properties can be gained from the obtained posterior distributions.

Keywords: Probabilistic parameter estimation, personalized modeling, Markov Chain Monte Carlo, Gaussian process.

1 Introduction

Patient-specific models are showing increasing promise in personalized medicine [15]. While advancement in medical imaging has made personalized geometrical models a reality, the challenge of obtaining patient-specific tissue properties in

the form of model parameters remains unresolved. These model parameters often cannot be directly measured, but have to be inferred from clinical data that are sparse and noisy.

Most existing works on parameter estimation use deterministic methods to find an *optimal* value of the model parameter so that model outputs best fit the measurement data [18,15,5]. However, significant uncertainty can exist in the estimated parameter values due to the uncertainty in available data. This important source of uncertainty will result in unknown variability in model outputs that, if left unquantified, will hinder their reliable adoptions. Additionally, over-parameterization and coupling between parameters may result in many parameter configurations that fit the data equally well. This issue of identifiability cannot be observed when only an *optimal* solution is being sought.

A probabilistic estimation of model parameters can address the above challenges by obtaining the posterior probability density (pdf) of the parameters conditioned on the data [14,8,9]. However, limited progress has been made in this direction because the posterior pdf comprises of a complex simulation model that are analytically intractable and computationally expensive. While Markov Chain Monte Carlo (MCMC) methods are natural choices for drawing samples from an analytically-intractable pdf, they become prohibitive in this context because the evaluation of each sample involves a model simulation that could take hours or even days for a single run. To address this critical challenge, an effective approach is to construct an efficient surrogate for the compute-intensive simulation model using methods such as polynomial chaos [8] and kriging [14]. These surrogate models can then replace the original model in the posterior pdf for substantially faster sampling [8,14]. However, this approach has two major limitations. First, the sampling is carried out on an approximated rather than the exact posterior pdf. Thus the efficiency is gained at the expense of sampling accuracy. Second, the surrogate is built to be accurate in important regions of the simulation model [8,14]. Thus the approximation accuracy can be limited in important regions of the posterior pdf, such as those of high probability.

We propose to overcome these issues by integrating surrogate modeling of the posterior pdf into the classic form of MCMC sampling to improve its acceptance rate. A similar idea was reported in [9], where a Gaussian process (GP) surrogate of the posterior pdf was constructed using hybrid Monte Carlo (HMC), the gradient of which was then used to find better proposals when sampling the exact posterior pdf. However, to construct the GP surrogate by random exploration of the sampling space, the number of model simulations needed increases exponentially with the number of unknown parameters. In addition, although the gradient of the GP surrogate allows a smarter exploration of the sampling space during HMC, the simulation model still needs to be probed at each proposed sample whereas a large portion of such heavy computation is spent at rejecting unwanted proposals. Important challenges remain in order to further reduce the number of model simulations needed in this type of approaches.

In this paper, we address these challenges from both the end of surrogate modeling and MCMC sampling. First, rather than a random exploration, we

quickly construct a GP surrogate of the posterior pdf by deterministic optimization favoring high accuracy in regions of high posterior probability. Second, we modify common proposal distributions in Metropolis Hastings (MH) sampling by first testing the acceptance of each proposal on the far-cheaper-to-evaluate GP surrogate, quickly rejecting a large number of proposals and allowing only those accepted by the surrogate to be tested by the exact pdf. Compared to directly sampling from an approximated pdf [8,14], the presented method ensures a high accuracy by generating the final samples from the exact distribution. Compared to directly sampling the exact pdf, the presented method reduces computation by avoiding expensive model simulations at unlikely proposals.

We evaluate the presented method on estimating tissue excitability of a cardiac electrophysiological model using non-invasive electrocardiogram (ECG) data. In synthetic experiments, we first evaluate the sampling accuracy and computational cost of the presented method against directly sampling the exact posterior pdf. Using the exact posterior pdf as a baseline, we then compare the accuracy of the presented method to an approach that, similar to existing work [14], samples only the surrogate posterior pdf. Finally, in both synthetic and real-data studies, we analyze the uncertainty, identifiability, and heterogeneity of tissue excitability using its posterior pdfs personalized from ECG data.

2 Cardiac Electrophysiological System

Whole-heart Electrophysiology Model: Simplified electrophysiological models are popular candidates for parameter estimation in personalized modeling [15]. They can reproduce the general shape of action potential with a small number of parameters and reasonable computation. As a preliminary demonstration of the presented method, we consider the two-variable *Aliev-Panfilov* (AP) model [2]:

$$\begin{aligned}\partial u/\partial t &= \partial/\partial x_i d_{ij} \partial u/\partial x_j - ku(u-a)(u-1) - uv, \\ \partial v/\partial t &= \varepsilon(u,v)(-v - ku(u-a-1)),\end{aligned}\tag{1}$$

where u is the action potential and v is the recovery current. Parameter d_{ij} is the conductivity, parameter ε controls the coupling between the recovery current and action potential, k controls the repolarization, and a controls the excitability of the myocyte. As a proof of concept, in this study we consider quantifying the uncertainty of parameter a because it is closely associated with the ischemic severity of the myocardial tissue and model output u is sensitive to its value.

The meshfree method as described in [17] is used to discretize and solve the AP model on the 3D myocardium. The direct estimation of parameter a at the resolution of the cardiac mesh is impossible due to non-identifiability and heavy computation. Instead, we consider the estimation of parameter a at a reduced dimension. Any appropriate dimension reduction method can be used. Here, we use a recently reported method that automatically groups spatial nodes of the cardiac mesh into 5 – 17 regions that are at various resolutions and that are most homogeneous in tissue properties [5,4].

Measurement Model: Spatio-temporal cardiac action potential produces time-varying ECG signals on the body surface. This relationship can be described by the quasi-static approximation of the electromagnetic theory [10]. Solving the governing equations on a discrete mesh of heart and torso [17], a linear model between ECG data \mathbf{Y} and action potential \mathbf{U} can be obtained as: $\mathbf{Y} = \mathbf{H}\mathbf{U}(\boldsymbol{\theta})$. Here, \mathbf{H} is the transfer matrix unique to each heart and torso geometry, and $\boldsymbol{\theta}$ is the vector of spatially-varying local parameters a at a reduced dimension.

3 Probabilistic Parameter Estimation

The relationship between parameter $\boldsymbol{\theta}$ and ECG data \mathbf{Y} can be expressed as:

$$\mathbf{Y} = F(\boldsymbol{\theta}) + \boldsymbol{\epsilon} \quad (2)$$

where F consists of the whole-heart electrophysiological model and the measurement model as described in section 2. $\boldsymbol{\epsilon}$ accounts for discrepancy between model outputs and measurement data. Using Bayes' theorem, the unnormalized posterior density of the model parameter $\boldsymbol{\theta}$ can be obtained as:

$$\pi(\boldsymbol{\theta}|\mathbf{Y}) \propto \pi(\mathbf{Y}|\boldsymbol{\theta})\pi(\boldsymbol{\theta}) \quad (3)$$

Assuming noise $\boldsymbol{\epsilon}$ to follow a zero mean Gaussian distribution with a diagonal covariance $\boldsymbol{\Sigma}_e = \sigma_e^2 \mathbf{I}$, the likelihood $\pi(\mathbf{Y}|\boldsymbol{\theta})$ can be formulated as:

$$\pi(\mathbf{Y}|\boldsymbol{\theta}) \propto \exp(-1/2\sigma_e^2 \|\mathbf{Y} - F(\boldsymbol{\theta})\|^2) \quad (4)$$

The prior distribution $\pi(\boldsymbol{\theta})$ quantifies prior knowledge over the parameter. Here we use a uniform distribution in bounded space $[0, 0.52]$ to include the minimal physiological knowledge about the range of values for this parameter: $a \sim 0.15$ represents normal excitability, while increased value represents increased loss of excitability until $a \sim 0.5$ represents necrotic tissue.

MCMC sampling of the posterior pdf in equation (3) is infeasible because the evaluation of each sample requires an expensive model simulation. Below we describe the presented method that accelerates MCMC sampling of (3) via the use of an efficient GP surrogate in the modification of proposal distributions.

GP Surrogate of Posterior Functions: GP is a popular method to model a function that lacks an explicit form or is difficult to evaluate. such as a deep learning model, an experiment to be designed, and a multiscale simulation model [12]. Here, we use it to approximate the exact posterior pdf in equation (3).

To initialize, we take a GP with a zero mean function and an anisotropic ‘‘Mat ern 5/2’’ co-variance function [12]:

$$\kappa(\boldsymbol{\theta}_1, \boldsymbol{\theta}_2) = \alpha^2 \{1 + \sqrt{5d^2(\boldsymbol{\theta}_1, \boldsymbol{\theta}_2)} + 5/3d^2(\boldsymbol{\theta}_1, \boldsymbol{\theta}_2)\exp(-\sqrt{5d^2(\boldsymbol{\theta}_1, \boldsymbol{\theta}_2)})\} \quad (5)$$

where $d^2(\boldsymbol{\theta}_1, \boldsymbol{\theta}_2) = (\boldsymbol{\theta}_1 - \boldsymbol{\theta}_2)^\top \boldsymbol{\Lambda}(\boldsymbol{\theta}_1 - \boldsymbol{\theta}_2)$, the diagonal of $\boldsymbol{\Lambda}$ are length scales, and α^2 is the co-variance amplitude. This kernel relaxes the assumption on the

smoothness of the posterior pdf compared to commonly-used squared exponential kernel. The GP is then learnt by an iteration of the following two steps:

1. *Finding optimal points to build the GP:* Sample points used to build the GP are placed so as to: 1) globally approximate the posterior pdf, and 2) concentrate more in regions of high posterior probability. For the former, points are chosen where the predictive uncertainty $\sigma(\boldsymbol{\theta})$ of the current GP is high (to facilitate exploration of uncertain space). For the latter, points are chosen where the predictive mean $\mu(\boldsymbol{\theta})$ of the current GP is high (to exploit current knowledge about the space of high posterior probability). This is done by finding the point that maximizes the upper confidence bound of the GP [12]:

$$\hat{\boldsymbol{\theta}} = \arg \max_{\boldsymbol{\theta}} \{ \mu(\boldsymbol{\theta}) + \beta^{1/2} \sigma(\boldsymbol{\theta}) \} \quad (6)$$

where $\mu(\boldsymbol{\theta})$ and $\sigma(\boldsymbol{\theta})$ are evaluated by the Sherman-Morrison-Woodbury formula [12]. The parameter β balances between exploitation and exploration of the sample space [12]. Equation (6) is optimized using Bound Optimization BY Quadratic Approximation (BOBYQA) [11].

2. *Updating the GP surrogate:* Once a new point is obtained, the exact posterior pdf (3) is evaluated at this point and the GP is updated. After every a few updates of the GP, we optimize the hyperparameters (length scales $\boldsymbol{\Lambda}$ and covariance amplitude α) by maximizing the marginal likelihood.

These two steps iterate until new points collected change little. In this way, we quickly obtain a surrogate $\pi^*(\boldsymbol{\theta}|\mathbf{Y})$ of the exact posterior pdf (3) that is much cheaper to evaluate and is most accurate in regions of high posterior probability.

MCMC Acceleration using GP Approximation: Metropolis Hasting (MH) is commonly used for generating a Markov chain of samples from a stationary distribution [1]. Supposing that the n^{th} sample in the Markov chain is $\boldsymbol{\theta}_n$, MH in its native form first draws a random candidate from a proposal distribution $q(\boldsymbol{\theta}|\boldsymbol{\theta}_n)$, and then accepts the candidate with an acceptance probability given as:

$$\rho(\boldsymbol{\theta}_n, \boldsymbol{\theta}) = \min\left(1, \frac{q(\boldsymbol{\theta}_n|\boldsymbol{\theta})\pi(\boldsymbol{\theta}|\mathbf{Y})}{q(\boldsymbol{\theta}|\boldsymbol{\theta}_n)\pi(\boldsymbol{\theta}_n|\mathbf{Y})}\right) \quad (7)$$

which means that the expensive posterior pdf (3) has to be probed — namely, the simulation model to be run — at every proposed sample. Because obtaining a proposal $q(\boldsymbol{\theta}|\boldsymbol{\theta}_n)$ similar to the exact posterior pdf is notoriously difficult [1,7], the acceptance rate is often low which leads to an infeasible amount of computation that will mainly be spent at rejecting unwanted proposals.

To improve the acceptance rate of MH, we use the much-faster-to-evaluate GP surrogate to modify commonly-used proposal distributions, such as a Gaussian distribution centered at $\boldsymbol{\theta}$ with covariance $\boldsymbol{\Sigma}_p = \sigma_p^2 \mathbf{I}$. A candidate sample $\boldsymbol{\theta}$ is first drawn from the proposal distribution as usual. Instead of directly testing the acceptance of this candidate using equation (7), we first test the acceptance of this candidate against the surrogate GP $\pi^*(\boldsymbol{\theta}|\mathbf{Y})$ using a probability ρ_A :

$$\rho_A(\boldsymbol{\theta}_n, \boldsymbol{\theta}) = \min\left(1, \frac{q(\boldsymbol{\theta}_n|\boldsymbol{\theta})\pi^*(\boldsymbol{\theta}|\mathbf{Y})}{q(\boldsymbol{\theta}|\boldsymbol{\theta}_n)\pi^*(\boldsymbol{\theta}_n|\mathbf{Y})}\right) \quad (8)$$

which is computationally much cheaper to evaluate compared to (7). Intuitively, this additional stage of acceptance or rejection modifies the proposal distribution by filtering out candidates that have a high probability of being rejected by the exact pdf. Only the candidates accepted by the GP surrogate are then evaluated against the exact posterior pdf for acceptance with a probability ρ_E :

$$\rho_E(\boldsymbol{\theta}_n, \boldsymbol{\theta}) = \min\left(1, \frac{\pi(\boldsymbol{\theta}|\mathbf{Y})\pi^*(\boldsymbol{\theta}_n|\mathbf{Y})}{\pi(\boldsymbol{\theta}_n|\mathbf{Y})\pi^*(\boldsymbol{\theta}|\mathbf{Y})}\right) \quad (9)$$

In this way, the acceptance rate is improved and unnecessary model simulations are avoided at proposals that would have been rejected with high probability. This is achieved without sacrificing sampling accuracy because the final Markov chain is generated via acceptance by the exact posterior pdf. Due to space limit, refer to [3,6] for discussions on the ergodicity and convergence of the Markov chain to the exact pdf when modifying the proposal using an approximation.

4 Experiments

Synthetic Experiments: On two image-derived human heart-torso models, we include six cases of infarcts of different sizes and locations of the LV. Note that a relatively small number of experiments is considered because it is time consuming to obtain samples on the exact posterior pdf as a baseline. For each synthetic case, parameter a in the AP model is set to be 0.15 for normal tissue and 0.5 for infarct tissue. 120-lead ECG is simulated and corrupted with 20dB Gaussian noise as measurement data. After dimensionality reduction [5], the number of parameters to be estimated in each case ranges from 9 to 12.

In all MH sampling, we use a four parallel chains with same Gaussian proposal distribution but four different initial points. Because the GP surrogate is efficient to sample, we use it to tune the variance of the proposal distribution and the starting point for each MCMC chain. The former is tuned to attain an acceptance rate of 0.3 – 0.4. For the latter, a rapid sampling of the GP surrogate is first conducted using slice sampling for 20,000 samples; assuming that these samples come from a mixture of four Gaussian distributions, the mean of each is then used to start each of the four parallel chains. After discarding initial burn-in samples and picking alternate samples to avoid auto-correlation in each chain, the samples from four chains are combined. The convergence of all MCMC chains are tested using trace plots, Geweke statistics, and Gelman-Rubin statistics [1,7].

Validation against exact posterior pdf: Fig. 1(a)-(b) presents examples of posterior pdfs obtained from two experiments where the dimension of unknown parameters are 9 and 10, respectively. As shown, the presented sampling strategy (green curve) closely reproduces true posterior pdf (red curve). In the mean time, it reduces the computational cost by an average of 53.56% (Fig. 1(c)) despite the overhead of constructing the GP surrogate which, as highlighted in the purple bar in Fig. 1(c), is negligible compared to the computation required for sampling.

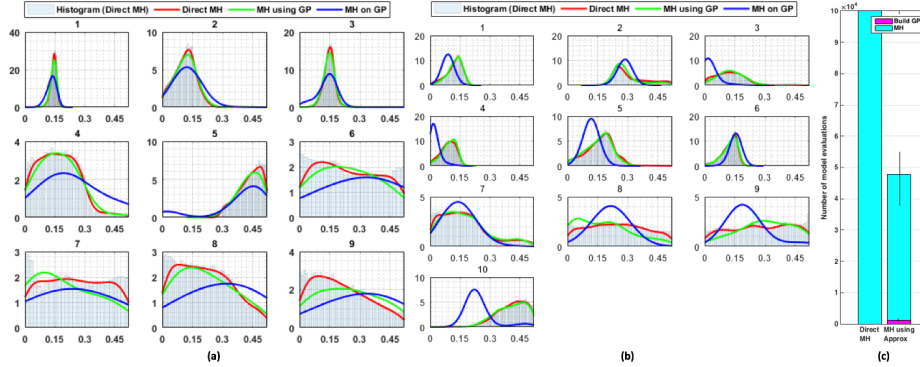


Fig. 1: (a)-(b): Examples of exact posterior pdfs (red) *vs.* those obtained by the presented method (green) and sampling the GP surrogate only (blue). (c): Comparison of efficiency in terms of the number of model simulations between the presented method (right bar) and sampling the exact posterior pdf (left bar).

Table 1: Absolute errors in mean, mode, and standard deviation against the exact posterior pdf: the presented method *vs.* directly sampling the GP surrogate.

	Mean	Mode	Standard deviation
Presented method	0.0154 ± 0.0186	0.0510 ± 0.0711	0.0059 ± 0.0074
Sampling surrogate	0.0549 ± 0.0532	0.0972 ± 0.1111	0.0309 ± 0.0306

Comparison with directly sampling the GP surrogate: Directly sampling the GP posterior pdf in replacement of the exact pdf, as commonly done in existing methods [14], requires significantly less computation because no model simulation is needed. However, the sampling accuracy is limited. This is especially evident in Fig. 1(b) where sampling the GP surrogate (blue curve) produces a distribution that is different from the exact pdf not only in general shape but also in locations of the mode. Using the mean, mode, and standard deviation (std) of the exact pdf as a baseline, Table 1 shows that sampling errors of the presented method are significantly lower than those from sampling the surrogate (paired *t*-test on 60 estimated parameters, $p < 0.0012$).

Analysis of uncertainty & identifiability: Fig. 2 shows maps of summary statistics obtained by the presented method in two cases with septal infarcts. In case 1, there are 7 regions of the heart to be parameterized. As shown, a strong false positive at the RV lateral wall is present at both the posterior mode and mean of the estimated parameters. The std map indicates that this false positive is associated with a high uncertainty. For a closer look at the reason for such uncertainty, Fig. 3 shows posterior pdfs of the estimated parameters (the region on which each parameter is estimated is shown in the first column, where green indicates a healthy region and red an infarcted region). As shown, the first three regions correspond to healthy regions and their parameters are estimated with a prominent single mode and low uncertainty. Regions 4 and 5 correspond to

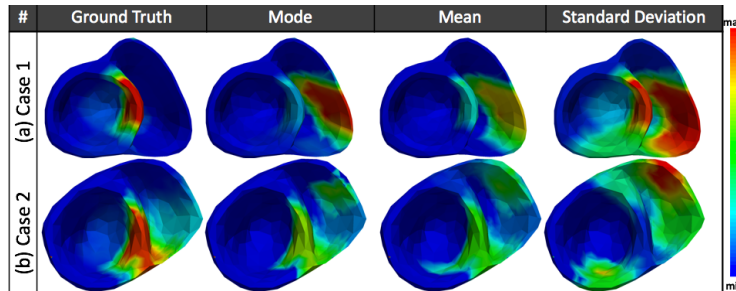


Fig. 2: Synthetic data: mean, mode and std of estimated posterior pdfs.

two small healthy regions close to the infarct. Their parameters are estimated accurately but with higher uncertainty. The last two regions correspond to the infarcted region and the RV wall. Their parameters show a coupling that results in a bimodal distribution. This also exhibits as a switching behavior in the trace plot of these two parameters (Fig. 3(c)): if the parameter of region 6 is estimated towards a healthier state, the parameter of region 7 would tend towards an infarcted state. Such switching property in Markov chains is associated with non-identifiability [16], *i.e.*, either combination of the two parameter values could fit the measurement data similarly well. Knowledge about this non-identifiability is valuable for placing proper trust in the obtained posterior point estimates.

In case 2, there are 11 regions to be parameterized, five of which along with their estimated parameter pdfs are shown in Fig. 4. As shown, the parameter of the region that contains the true infarct (a) is correctly estimated with a narrow uni-modal distribution. In comparison, several RV regions adjacent to the septal infarct (b-e) have difficulty converging which we suspect could be again caused by non-identifiability. As a result, we obtain a solution where the true septal infarct is estimated with high confidence, whereas the false positives are associated with a higher uncertainty as summarized in Fig. 2. Namely, uncertainty analysis helps differentiate false positives from true positives in this case.

Real-data Experiments: We conduct real-data studies on three patients who underwent catheter ablation of ventricular tachycardia due to prior infraction [13]. Patient-specific heart-torso geometrical models are obtained from axial CT images. The uncertainty of tissue excitability in the AP model (1) is estimated from 120-lead ECG data. For evaluation of the results, bipolar voltage data from *in-vivo* catheter mapping are used. However, it should be noted that voltage maps are not a direct measure of tissue excitability and thus should be interpreted as a reference but not the validation data. Fig. 5 shows the catheter data along with the estimation results, where the first column shows the original voltage maps (red: dense scar $\leq 0.5\text{mV}$; purple: healthy tissue $> 1.5\text{mV}$; green: scar border $0.5 - 1.5\text{mV}$) and the second column shows the same voltage data registered to CT-derived cardiac meshes. As shown, compared to synthetic data, a real infarct is often distributed with higher heterogeneity. The resolution to

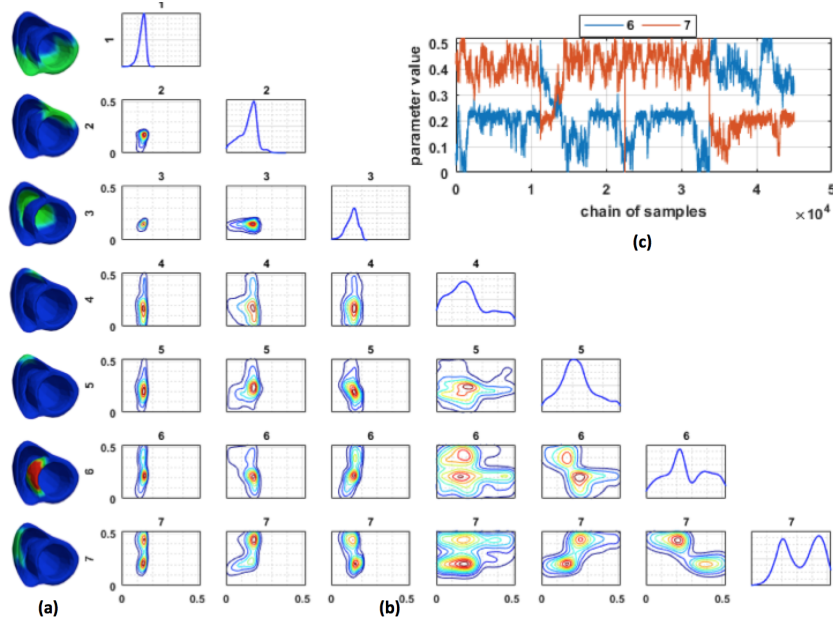


Fig. 3: (a) Regions of heart to be parameterized (red: infarct, green: non-infarct/mixed). (b) Uni-variate and bi-variate marginal pdf plots. (c) Trace plot for parameters of regions 6 and 7 showing switching behavior.

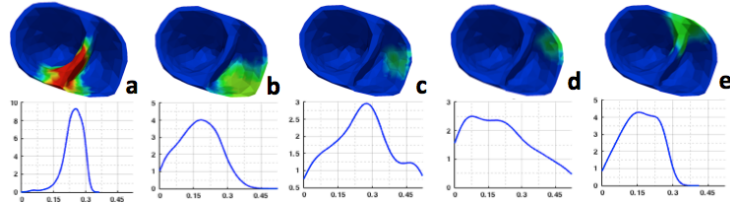


Fig. 4: Uni-variate marginal probability density plots and the corresponding regions of heart to be parameterized for case 2 from Fig. 2.

which such heterogeneity can be captured is largely limited by the method of dimensionality reduction. Below we show how uncertainties of the lower-resolution estimation are associated with the heterogeneity of the underlying tissue.

Case 1: The voltage data for case 1 (Fig. 5(a)) shows a dense infarct at inferolateral LV with a heterogeneous region extending to lateral LV. Dimensionality reduction generates 12 regions of the heart to be parameterized, five of which are listed in Fig. 6 along with the estimated posterior marginal pdfs for their parameters. As shown, the parameter for the region of infarct core (a) is correctly estimated with low uncertainty. For several regions around the heterogeneous infarct border (b-d), uncertainties of the estimation become higher. A particularly

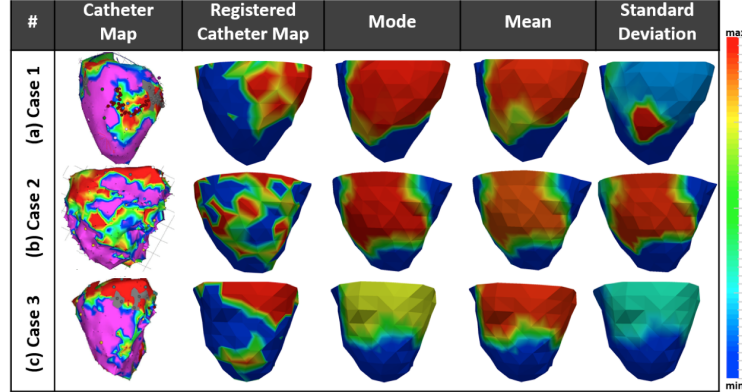


Fig. 5: Real-data experiments: mean, mode and std of posterior pdfs.

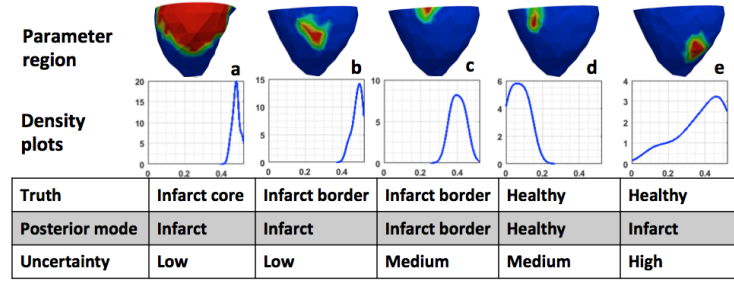


Fig. 6: Real-data experiments: marginal probability density plots and the corresponding regions of heart being parameterized in case 1.

high uncertainty is obtained at a small healthy region by the scar border (e), where the parameter is incorrectly estimated. This produces an estimation with correct posterior mode/mean and low uncertainty at the infarct core, increased uncertainty at the heterogeneous infarct border, and high uncertainty at a region of false-positive near the infarct border as summarized in Fig. 5(a).

Case 2: The voltage data for case 2 (Fig. 5(b)) shows a massive yet quite heterogeneous infarct at lateral LV. Dimensionality reduction generates 8 regions of the heart to be parameterized, five of which are listed in Fig. 7 along with the estimated posterior marginal pdfs for their parameters. As shown, for healthy regions remote from the infarct (a-b), their parameters are correctly estimated with high confidence. For healthy regions close to the infarct (c-d), their parameters are correctly estimated but with lower confidence. For the region that corresponds to the infarct (e), its abnormal parameter is correctly captured but with a high uncertainty – likely reflecting the heterogeneous nature of tissue properties in this region. As summarized in Fig. 5(b), while the estimation correctly reveals the region of infarct as in case 1, it is also associated with a higher uncertainty compared to the less heterogeneous infarct in case 1.

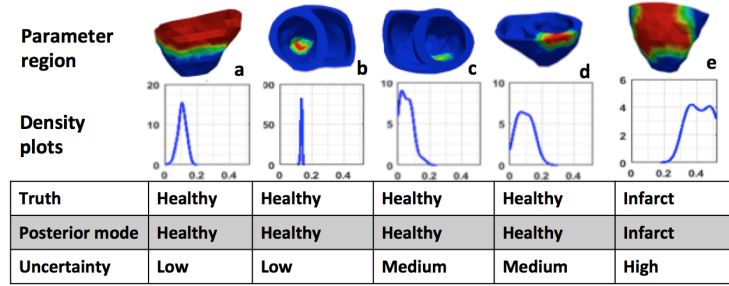


Fig. 7: Real-data experiments: marginal probability density plots and the corresponding regions of heart being parameterized in case 2.

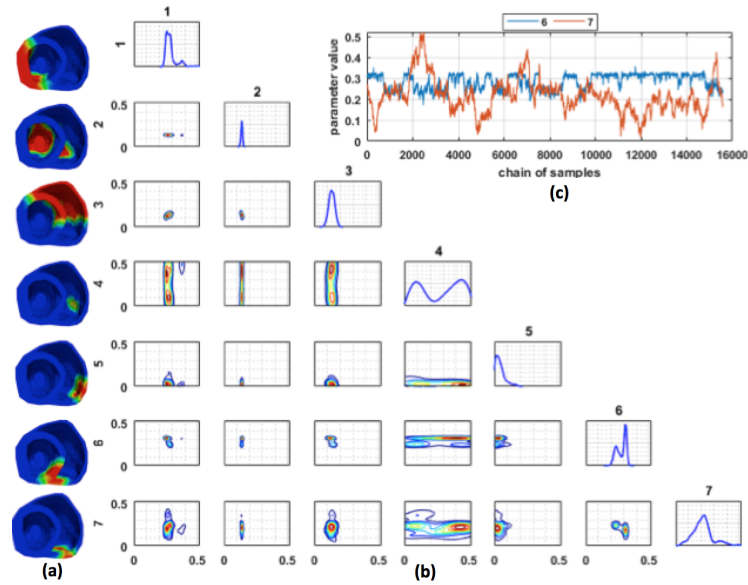


Fig. 8: Real-data experiments for case 3. (a) Regions of heart to be parameterized. (b) Uni-variate and bi-variate marginal pdf plots. (c) Trace plot for parameters of regions 6 and 7.

Case 3: The catheter data for case 3 (Fig. 5(c)) shows low voltage at lateral LV and RV, although it was not clear whether the low voltage on lateral RV was due to an infarct or fat layer. As shown in Fig. 8, there are 7 regions of the heart to be parameterized. The abnormal parameter in lateral LV (region 1) is estimated with a narrow uni-modal distribution. In contrast, the marginal distribution for the parameter in lateral RV (region 4) shows a bimodal distribution with one mode in healthy range and the other in infarcted range. Markov chains for the parameters of two nearby regions at RV (regions 6-7) also show a switching

behavior (Fig. 8(c)). This produces an estimate of abnormal tissue property with high confidence at lateral LV (Fig. 5(c)), and less confidence at lateral RV.

5 Conclusion

This paper presents a novel approach to efficiently yet accurately sample the distribution of parameters in complex simulation models. This is achieved by using GP-based surrogate modeling to improve the proposal distribution. A more accurate GP surrogate of the posterior pdf is more expensive to build but more effective in improving the acceptance rate of MH sampling, while a less accurate GP surrogate is faster to build but less effective in accelerating MH sampling. How to maintain this balance is to be investigated in future works.

Acknowledgments. This work is supported by the National Science Foundation under CAREER Award ACI-1350374 and the National Institute of Heart, Lung, and Blood of the National Institutes of Health under Award R21HL125998.

References

1. Adrieu, C., Freitas, N., Doucet, A., Jordan, M.: An introduction to markov chain monte carlo for machine learning. *Machine Learning* 50 (2003)
2. Aliev, R.R., Panfilov, A.V.: A simple two-variable model of cardiac excitation. *Chaos, Solitons & Fractals* 7(3), 293–301 (Mar 1996)
3. Christen, J.A., Fox, C.: Markov chain monte carlo using an approximation. *Journal of computational and graphical statistics* (2012)
4. Dhamala, J., Arevalo, H.J., Sapp, J., Horacek, M., Wu, K.C., Trayanova, N.A., Wang, L.: Spatially adaptive multi-scale optimization for local parameter estimation in cardiac electrophysiology. *IEEE TMI* 36(9), 1966–1978 (2017)
5. Dhamala, J., Sapp, J.L., Horacek, M., Wang, L.: Spatially-adaptive multi-scale optimization for local parameter estimation: Application in cardiac electrophysiological models. In: *MICCAI*. pp. 282–290. Springer (2016)
6. Efendiev, Y., Hou, T., Luo, W.: Preconditioning markov chain monte carlo simulations using coarse-scale models. *SIAM Journal on Scientific Computing* 28(2), 776–803 (2006)
7. Gilks, W.R., Richardson, S., Spiegelhalter, D.: *Markov chain Monte Carlo in practice*. CRC press (1995)
8. Konukoglu, E., et al.: Efficient probabilistic model personalization integrating uncertainty on data and parameters: Application to eikonal-diffusion models in cardiac electrophysiology. *Progress in biophysics and molecular biology* 107(1) (2011)
9. Lê, M., Delingette, H., Kalpathy-Cramer, J., et al.: Bayesian personalization of brain tumor growth model. In: *MICCAI*, 2015
10. Plonsey, R.: *Bioelectric phenomena*. Wiley Online Library (1969)
11. Powell, M.J.: Developments of newuoa for minimization without derivatives. *IMA journal of numerical analysis* 28(4), 649–664 (2008)
12. Rasmussen, C.E.: *Gaussian processes for machine learning* (2006)
13. Sapp, J., Dawoud, F., Clements, J., Horáček, M.: Inverse solution mapping of epicardial potentials: Quantitative comparison to epicardial contact mapping. *Circulation: Arrhythmia and Electrophysiology* pp. CIRCEP–111 (2012)

14. Schiavazzi, D., Arbia, G., Baker, C., et al.: Uncertainty quantification in virtual surgery hemodynamics predictions for single ventricle palliation. *International journal for numerical methods in biomedical engineering* (2015)
15. Sermesant, M., Chabiniok, R., Chinchapatnam, P., et al.: Patient-specific electromechanical models of the heart for the prediction of pacing acute effects in crt: A preliminary clinical validation. *Medical image analysis* 16(1), 201–215 (2012)
16. Siekmann, I., Sneyd, J., Crampin, E.J.: Mcmc can detect nonidentifiable models. *Biophysical journal* 103(11), 2275–2286 (2012)
17. Wang, L., Zhang, H., Wong, K.C., Liu, H., Shi, P.: Physiological-model-constrained noninvasive reconstruction of volumetric myocardial transmembrane potentials. *IEEE Trans Biomed Eng* 57(2), 296–315 (2010)
18. Wong, K., Relan, J., et al.: Strain-Based regional nonlinear cardiac material properties estimation from medical images. In: *MICCAI 2012*. Springer (2012)